Available online at www.sciencedirect.com
ScienceDirect
Acta Materialia 58 (2010) 4414–4423
Acta MATERIALIA
www.elsevier.com/locate/actamat

Abnormal grain growth of Goss grains in Fe–3% Si steel driven by sub-boundary-enhanced solid-state wetting: Analysis by Monte Carlo simulation

Kyung-Jun Ko [a], Anthony D. Rollett [b], Nong-Moon Hwang [c,*]

[a] Electrical Steel Sheet Research Group, Technical Research Laboratories, POSCO, Pohang 790-785, Republic of Korea
[b] Materials Science and Engineering Department, Carnegie Mellon University, Pittsburgh, PA 15213, USA
[c] Department of Materials Science and Engineering and NRL of Charged Nanoparticles, Seoul National University, Seoul 151-742, Republic of Korea

Received 20 January 2010; received in revised form 1 April 2010; accepted 26 April 2010
Available online 18 May 2010

Abstract

The selective abnormal grain growth (AGG) of Goss grains in Fe–3% Si steel was investigated using a parallel Monte Carlo (MC) simulation based on the concept of sub-boundary-enhanced solid-state wetting. Goss grains that contain low angle sub-boundaries will induce solid-state wetting against grain boundaries in the matrix that exhibit a moderate variation in grain boundary energy, as expected from the variation in boundary type. AGG generates a sharp Goss texture provided that only Goss-oriented grains have the required sub-grain structure to grow selectively by sub-boundary-induced wetting and that other orientations lack the required content of low angle boundaries. This behavior is shown in three-dimensional MC simulations of microstructure evolution with textures and grain boundary distributions matched to experimental data.

Keywords: Grain boundary energy; Abnormal grain growth; Secondary recrystallization; Monte Carlo techniques; Simulation

1. Introduction

Abnormal grain growth (AGG) takes place in many metallic systems, especially after primary recrystallization of deformed polycrystals. AGG is often called secondary recrystallization because it changes the orientation and the grain size discontinuously from the microstructure remaining after primary recrystallization. In some materials, AGG is undesirable because it significantly degrades mechanical properties. However, in Fe–3% Si steel, which is used as a transformer material, AGG is utilized to optimize the magnetic properties. In this alloy, the grains near the so-called Goss orientation {1 1 0}<0 0 1> selectively undergo AGG and a strong Goss texture develops during secondary recrystallization. This phenomenon has remained a puzzle since it was first reported by Goss in 1935 [1].

In ceramics there is good evidence for changes in composition and consequently atomic structure in boundaries leading to AGG [2], but there is no evidence for such changes in Fe–3% Si [3]. AGG has been successfully explained in many ceramic systems, usually with thin liquid films, by growth via two-dimensional nucleation on the singular interface [4]. Also, in some highly textured specimens, where most grains have similar misorientations with low angle grain boundaries of low mobility, a grain with quite different misorientations with other grains will have exclusively high-mobility boundaries and grow abnormally [5]. The AGG treated in this paper does not apply to systems with a liquid phase or with a strong texture, but is limited to the metallic systems which typically occur during secondary recrystallization of metals.

Since Goss's paper, many studies have been published on the mechanism of selective Goss AGG in Fe–3% Si steel

* Corresponding author. Tel.: +82 2 880 8922; fax: +82 2 885 3292.
E-mail address: nmhwang@snu.ac.kr (N.-M. Hwang).

1359-6454/$36.00 © 2010 Acta Materialia Inc. Published by Elsevier Ltd. All rights reserved.
doi:10.1016/j.actamat.2010.04.038

because of its technical importance. In particular, precipitates such as MnS and AlN in Fe–3% Si steel are well known to play a critical role in AGG [6] by pinning the matrix grains. May and Turnbull [7] demonstrated that AGG does not occur without such precipitates. Most other explanations [8–10] for the selective Goss AGG are based on differences in grain boundary mobilities between the perimeters of Goss grains and all other grains. They assumed that abnormally growing grains have a large fraction of high-mobility boundaries that are less effectively pinned by precipitates compared with the other grains. Two hypotheses could possibly explain the origin of high-mobility boundaries: one ascribes the postulated mobility differences to variations in the frequency of certain coincidence site lattice (CSL) boundaries [8,9], whereas, according to the other model, intermediate misorientation boundaries have high energies [10]. However, conclusive experimental evidence to support one model over the other is lacking [11,12].

In complete contrast to the previous suggestions, a sub-boundary-enhanced wetting mechanism for selective Goss AGG has been suggested by Hwang et al. [13–17]. The three-dimensional morphology of solid-state wetting is illustrated in Fig. 1. Consider the potential for solid-state wetting along a triple junction at a quadruple point where four-grains are in contact (Fig. 1a). If grain "A" induces solid-state wetting along the triple junction of three grains, "B", "C" and "D", then the wetting grain "A" can be projected as shown in Fig. 1b, which shows a three-sided grain with negative grain boundary curvatures [18]. Therefore, if the sum of the inner angles is less than 180°, which is the criterion for triple junction wetting [19], grain "A" will wet the triple junction and penetrate between the other three grains.

If "A" grain shares a sub-boundary of very low energy with one of the other three grains, the energetic condition for triple junction wetting at quadruple junction is much more easily satisfied than in the absence of a sub-boundary. Therefore, if grain "A" shares a low angle misorientation with the other grains, together they will increase the probability of growing by sub-boundary-enhanced wetting. Recently, Ko et al. [16] and Lee et al. [17] used phase-field model and MC simulation, respectively, to show that grains with sub-boundaries of very low energy induce sub-boundary-enhanced solid-state wetting, and grow abnormally.

Experimentally, sub-boundaries with very low misorientations of less than 0.5° inside Goss grains in Fe–3% Si steel have been observed by Park et al. [20] and Ushigami et al. [21,22]. Doner et al. [23,24] also observed very low angle grain boundaries with misorientation less than 1° within primary recrystallized Goss grains. Recent experimental confirmation by Park et al. [20] based on extensive transmission electron microscopy observations showed that only abnormally growing Goss grains have sub-boundaries whereas other grains do not. Besides, Ko et al. [18] reported direct evidence of three-dimensional wetting morphology at the growth front of Goss AGG from serial section images. These results strongly support the sub-boundary-enhanced solid-state wetting mechanism, which explains the selection of the Goss component during AGG. The purpose of this study is to examine AGG by sub-boundary-enhanced solid-state wetting of the matrix by a Goss-oriented grain that contains sub-boundaries of

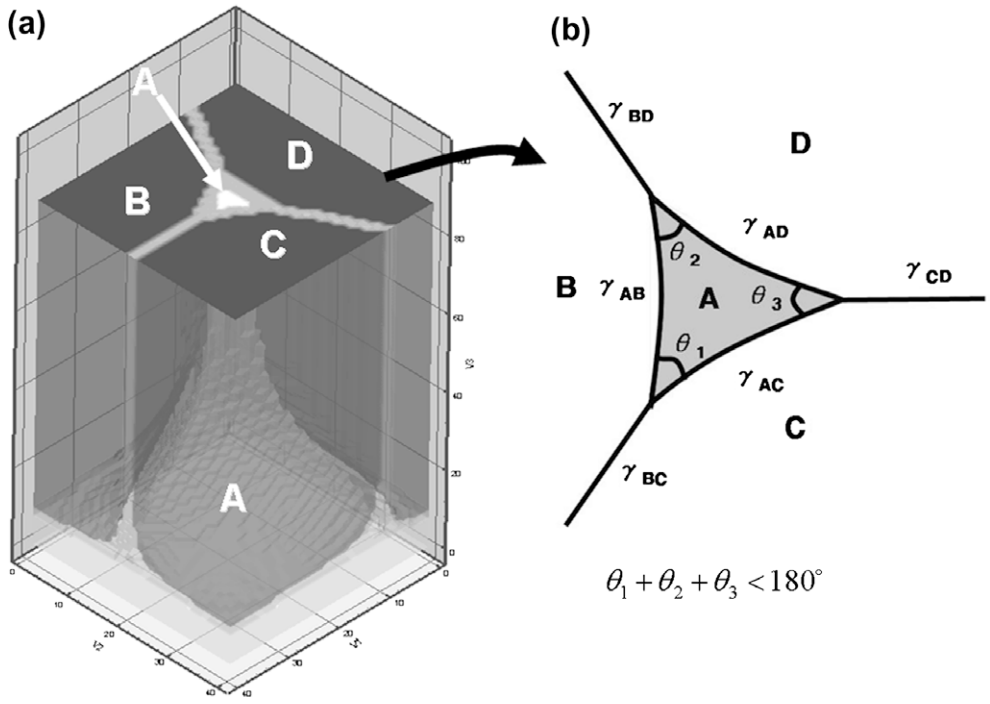

Fig. 1. (a) 3-D morphology of solid-state wetting and 2-D section vertical to the wetting direction. (b) Schematic drawing projecting the dihedral angles of grains "B" and "C", grains "C" and "D" and grains "B" and "D".

very low misorientation. Various degrees of anisotropy of grain boundaries in the matrix are simulated using parallel MC simulations of 3-D grain growth in 3-D microstructures with textures and grain boundary character fitted to measurements.

2. Monte Carlo simulation method

MC simulation of 3-D grain growth was performed on a 3-D simple cubic lattice using a code originally developed at the Sandia National Laboratories [25]. Each site or voxel has its own number, S_i, that represents the crystallographic orientation at that location, so that if adjacent sites have the same number, they are considered to belong to the same grain. Conversely adjacent sites that have different numbers are considered to be separated by a grain boundary. The range, Q, of S_i is assigned to be large enough so that the rate of coalescence events between grains during grain growth simulation is negligible; in these simulations, $Q = 10{,}000$.

The lattice site energy is given by the following sum over the sites:

$$E_i = \sum_{nn} J(S_i, S_j)[1 - \delta_{ij}] \tag{1}$$

where nn is the number of nearest neighbors (26 for third nearest neighbors in the simple cubic lattice), $J(S_i, S_j)$ is the grain boundary energy, S_i is the orientation of site i and δ_{ij} is the Kronecker delta function.

The grain boundary energy function, $J(S_i, S_j)$, incorporates the anisotropic grain boundary properties, which are assumed to depend on the misorientation angle between the two orientations S_i and S_j. Each orientation number, S_i, is assigned a corresponding set of Euler angles (φ_1, Φ, φ_2). The minimum misorientation is calculated by taking account of crystal symmetry. In the low misorientation angle regime ($\theta < \theta_{RS}$, where θ_{RS} is assigned 15° as the high misorientation angle cutoff), the grain boundary energy varies based on the dislocation model derived by Read and Shockley [26]. For high misorientation angles ($\theta \geqslant \theta_{RS}$), the dislocation model is no longer appropriate due to the overlap of dislocation cores. The grain boundary energy for high misorientation angles is expected to be approximately constant, but will depend in detail on both the boundary misorientation and the plane, i.e. on the complete grain boundary character distribution [27]. In the MC model, however, only variations in energy with misorientation can be easily accommodated because of the additional computational effort associated with determining boundary normals. Significant deviations from high energy are expected to occur near certain CSL boundaries, such as the $\Sigma 3$ [28]. Accordingly, the grain boundary energy in the high misorientation angle regime is assigned a random value in the range $1.0–1.0 + \alpha$ to model the variation in energy, where α is small compared to one. The energy of CSL boundaries up to $\Sigma 11$ is assumed to be low. The CSL boundaries are determined with the Brandon criterion, $v_m = \theta_{RS}/\Sigma^{1/2}$ [29]. The variation in energy at a CSL boundary is modeled with the Read–Shockley function [30].

The grain boundary energy function is given by

$$J(S_i,S_j) = \begin{cases} \frac{\theta}{\theta_{RS}}[1 - \ln(\frac{\theta}{\theta_{RS}})], & \theta < \theta_{RS} \quad \text{(low angle boundary)} \\ r', & \theta \geqslant \theta_{RS} \quad \text{(high angle boundary)} \\ \frac{w}{v_m}[1 - \ln(\frac{w}{v_m})], & \frac{w}{v_m} < 1 \quad \text{(CSL boundary)} \end{cases} \tag{2}$$

where θ is the misorientation angle between orientations S_i and S_j. θ_{RS} is assigned to be 15° as the high misorientation angle cutoff. r' is a random value in the range $1.0–1.0 + \alpha$ for an energy variation [16,17]. w is the deviation between the grain boundary and CSL boundary. The minimum energy of a CSL boundary, i.e. the minimum in the cusp, is limited to 0.5. All grain boundaries are assumed to have isotropic boundary mobility of 1.0 in this MC simulation.

In order to simulate the 3-D grain growth in this study, MC simulation is run in parallel mode by using the message passing interface [25]. The kinetics of grain growth is simulated by MC techniques where a site is selected at random and a candidate index is chosen from the set of neighbor indices. The probability for a reorientation to a candidate index, P, is given by

$$P(\Delta E) = \begin{cases} 1, & \Delta E \leqslant 0 \\ \exp(-\frac{\Delta E}{J(S_i,S_j)k_bT}), & \Delta E > 0 \end{cases} \tag{3}$$

where ΔE is the energy change associated with the change in orientation, k_b is Boltzmann's constant and T is the lattice temperature. In these simulations, the lattice temperature ($=k_bT$) was set at 1.2. Typical simulations with 180^3 lattices were done until 1000 MCS, which took about 10 min, using four parallel machines with Intel Xeon (R) CPU 3.00 GHz with the compiler of mpif77.

2.1. Initial microstructure of MC simulation for AGG by sub-boundary-enhanced solid-state wetting

In order to simulate sub-boundary-enhanced AGG in an Fe–3% Si sheet, the initial microstructure is constructed as follows. The initial microstructure (Fig. 2), which is a $180 \times 180 \times 180$ cubic lattice with periodic boundary conditions, was generated by MC grain growth simulation under isotropic grain boundary conditions. The initial microstructure has 15,506 grains, with a grain size distribution characteristic of normal grain growth. In order to incorporate the experimentally observed texture and grain boundaries into the initial microstructure for MC simulation, the orientations of each grain were rearranged to have the same orientation distribution function (ODF) and misorientation distribution function (MDF) as determined experimentally in the Fe–3% Si sheet. For a target ODF and MDF, orientation image mapping on 1/4 depth surface of a primary recrystallized Fe–3% Si sheet was obtained by electron backscattered diffraction. To assign orientations in the 3-D microstructure, we used a simulated

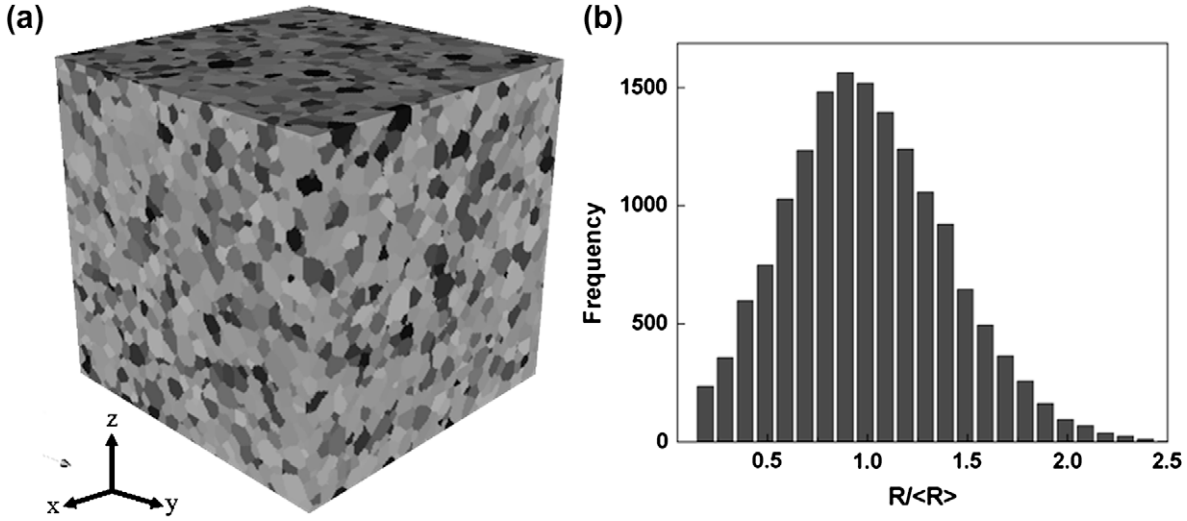

Fig. 2. (a) 3-D image of polycrystalline microstructure for MC simulation. (b) Grain size distribution of the initial microstructure.

annealing method to match the ODF and MDF simultaneously [27,31]. Fig. 3a and b shows the experimentally obtained and constructed MDF and ODF, respectively. The root mean square errors of ODF and MDF between the fitted distributions and the target data are less than 1.0×10^{-6}. The memory load during the preparation of the initial microstructure limits the system size of MC simulation to the 180^3 lattices and 15,806 grains.

A near-Goss-oriented grain (hereafter called a near-Goss grain), which has the smallest misorientation angle from the exact Goss orientation, was selected from the initial microstructure data set as a candidate for AGG. Since the size of the near-Goss grain was too small to grow by itself, the orientations of three neighbor grains in contact with the near-Goss grain were replaced by that of the near-Goss grain, thereby effectively increasing the size of the chosen grain. Such neighbor grains were selected in the order of the largest grain boundary area with the original near-Goss grain. After replacement the (linear) size of the near-Goss grain was 1.76 times larger than the average grain size.

In order to make the near-Goss grain contain sub-grain boundaries with a low enough misorientation angle to induce the expected wetting behavior, it is split into seven equal-sized sub-grains parallel to the z-axis. To obtain a specified misorientation angle, $\theta°$, between each sub-grain and the near-Goss grain, the orientations of the sub-grains within it were varied by $+\theta°$ or $-\theta°$ in φ_1, Φ or φ_2 (Euler angles) from the orientation of the parent Goss grain. The microstructures of the near-Goss grain and the orientations of the sub-grains are shown in Fig. 4.

3. MC simulation results and discussion

3.1. Abnormal grain growth by sub-boundary-enhanced solid-state wetting in MC simulation

In order to examine the effect of sub-boundaries inside the near-Goss grain on AGG, the MC simulations were performed for the near-Goss grain with and without sub-grains, as shown in Fig. 4. The values of θ (misorientation angle between the near-Goss grain and sub-grains) and α (energy anisotropy of high angle boundaries in the matrix) were set to be 0.05 and 0.2, respectively. Sequences of evolving microstructures for the near-Goss grains without and with sub-grains are shown in Fig. 5a and b, respectively. The near-Goss grains are indicated by a dotted line for 0 MCS of Fig. 5a and b. The near-Goss grain in Fig. 5a has no sub-grain, whereas the near-Goss grain in Fig. 5b has seven, which have misorientation angles of 0.05° with the near-Goss grain.

The near-Goss grain without sub-grains in Fig. 5a shrank slightly after 50 and 100 MCS and then disappeared, consumed by other grains after 200 MCS. However, the near-Goss grain with sub-grains in Fig. 5b continued to grow abnormally after 50 MCS. Most of the surface of the near-Goss grain in Fig. 5b, which corresponds to the grain boundary with the matrix grains, consists of different sub-grains, shown by different colors, which indicates that none of the sub-grains shrank but instead continued to grow. Therefore, sub-grain boundaries do not disappear but continue to grow, persistently and exclusively providing the growth advantage for the near-Goss grain. It should be noted that, in this simulation, the grain boundaries between the near-Goss grain and the matrix grains are not given any growth advantage, such as high mobility and low energy, as classically required for AGG [32].

3.2. Effect of the misorientation angle of sub-boundaries and the energy anisotropy of grain boundaries on the AGG by sub-boundary-enhanced solid-state wetting

In order to examine the effect of varying the misorientation angle of the sub-boundaries inside the near-Goss grain on AGG, MC simulations were performed for the near-Goss grain with sub-grains with misorientations (θ) that

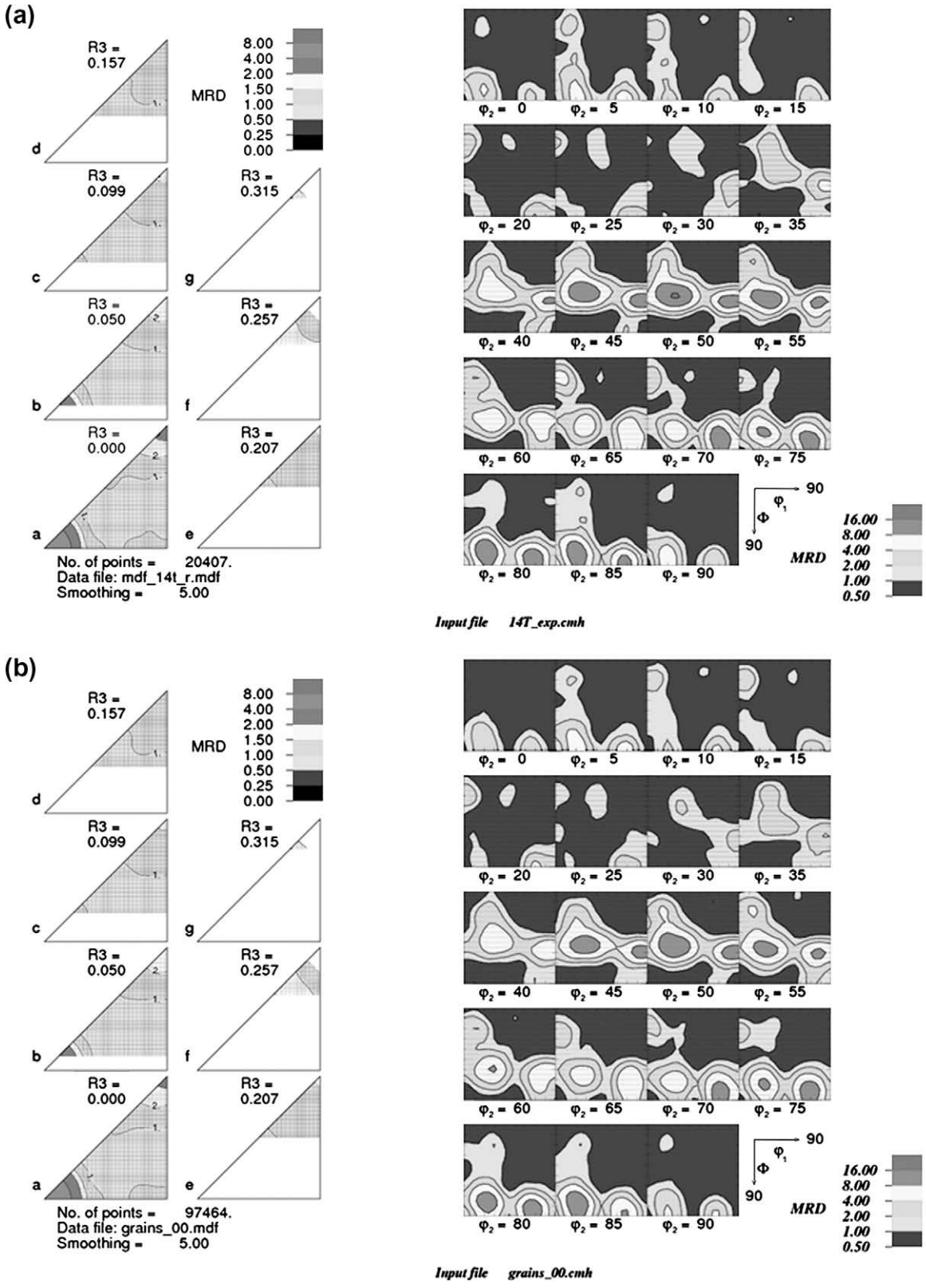

Fig. 3. MDF plot (ρ_3 slices through Rodrigues–Frank space) and ODF plot (φ_2 slices through Euler space) from (a) experimentally observed texture and (b) rearranged texture by the ODF and MDF matching code.

varied from 0.05° to 0.25°. In order to make a clearer judgement as to whether the near-Goss grain should grow abnormally or not by sub-boundary-enhanced wetting, we used a common criterion (see e.g. [32,33]), $d(R/\langle R\rangle)/dt > 0$, for AGG. Fig. 6 shows the size ratio of the near-Goss grain to the average size of matrix grains, $R/\langle R\rangle$,

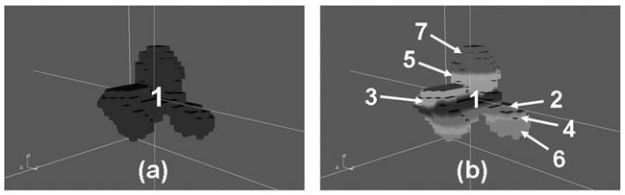

Number of sub-grain	Orientations (Euler angles)		
	ϕ_1	Φ	ϕ_2
1	179.88°	44.56°	183.17°
2	179.88°	44.56–Θ°	183.17°
3	179.88°	44.56+Θ°	183.17°
4	179.88°	44.56°	183.17–Θ°
5	179.88°	44.56°	183.17+Θ°
6	179.88–Θ°	44.56°	183.17°
7	179.88+Θ°	44.56°	183.17°

(c)

Fig. 4. The sub-grain microstructures inside the near-Goss grain (a) without sub-grain and (b) with six sub-grains. (c) The orientations of sub-grains for the near-Goss grain and sub-grains. The misorientation, θ, represents the angle between the near-Goss grain and sub-grains.

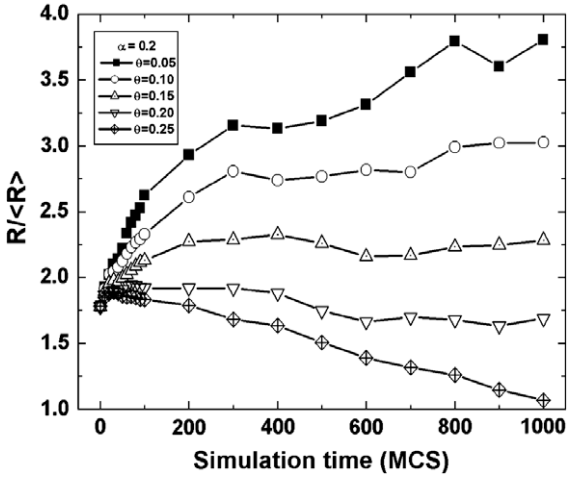

Fig. 6. Graphs of $R/\langle R\rangle$ vs. simulation time for the near-Goss grain with sub-grains whose sub-boundaries with the near-Goss grain have misorientation $\theta = 0.05°$, 0.10°, 0.15°, 0.20° and 0.25°. The energy anisotropy of high energy grain boundaries α is 0.2.

vs. simulation time for $\theta = 0.05°$, 0.10°, 0.15°, 0.20° and 0.25°, and the other conditions were fixed as the near-Goss grains with sub-grains and $\alpha = 0.2$. In Fig. 6, the overall slopes for $\theta = 0.05$ and 0.10° were positive, whereas the overall slopes for $\theta = 0.20$ and 0.25° were negative. The slope for $\theta = 0.15°$ was close to zero, indicating that this condition was at the boundary between normal and abnormal grain growth. Fig. 6 indicates that a lower misorientation angle of sub-boundaries inside the near-Goss grain gives it a higher growth rate, whereas a near-Goss grain with a higher misorientation angle ($\theta > 0.20°$) of sub-boundaries did not grow abnormally. These results show that in order to induce AGG by sub-boundary-enhanced solid-state wetting the misorientation angle of sub-grain boundaries must be lower than a certain threshold angle for inducing AGG, i.e. $\theta \approx 0.15°$ in this condition. These results correspond well with previous results obtained from PFM simulation [16]. The reason why the growth behavior is sensitive to such small changes in the misorientation angle is that the wetting probabilities for $\theta = 0.05°$ and 0.10° are higher than 1/3 and those for $\theta = 0.15°$, 0.20° and 0.25° are lower than 1/3. The details will be explained later (see Fig. 10).

The change in the distribution of grain boundary energies of matrix grains during grain growth is plotted in Fig. 7. The high misorientation ($\theta > 15°$) boundaries were uniformly distributed with energies between 1.0 and 1.2 at the start of each simulation. The frequency of high energy boundaries decreased abruptly soon after beginning a simulation (10 MCS), whereas the frequencies of boundaries with an energy of 1.0, which is the lowest energy

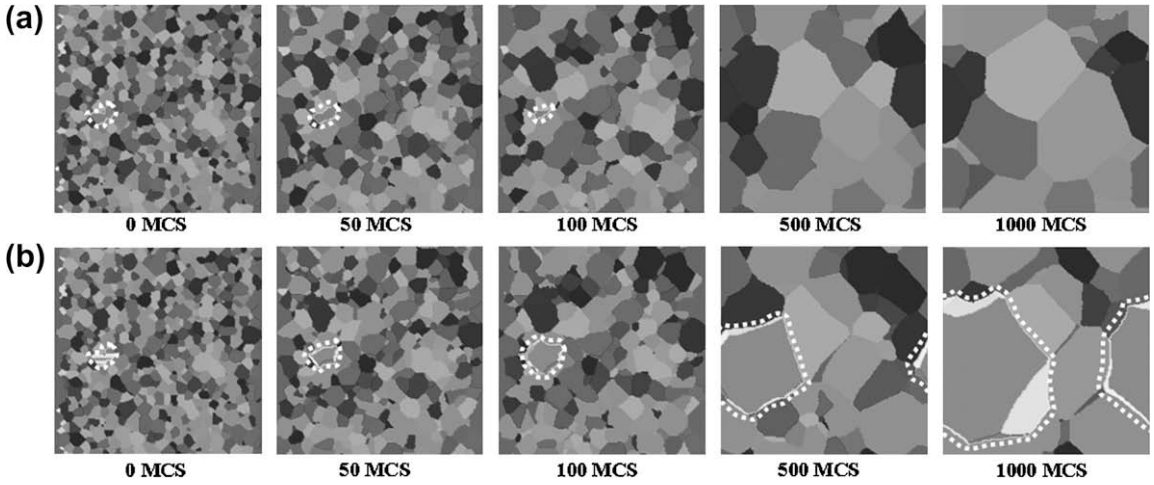

Fig. 5. The cross-sections of 3-D microstructure at $y = 63$ under the condition of the near-Goss grains (a) without sub-grain and (b) with sub-grains. θ (misorientation angle between sub-grains) and α (energy anisotropy of high angle boundary) are 0.05 and 0.2, respectively. The near-Goss grains are highlighted by white-dotted line.

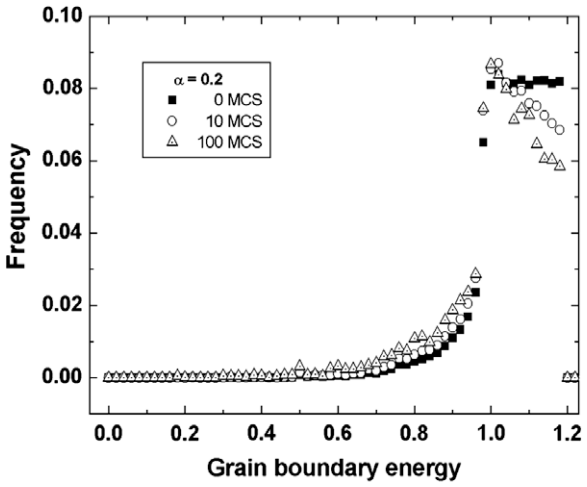

Fig. 7. The change of grain boundary energy distributions in the matrix grains during MC simulation for $\alpha = 0.2$.

among high misorientation boundaries, remain approximately constant; the frequency of low energy boundaries (<1.0) increased gradually. These changes of the grain boundary distribution in Fig. 7 indicate that most of the high energy boundaries that were present in the initial state (0 MCS) tended to disappear soon after grain growth started. These results show that, during grain growth, higher energy boundaries are replaced by lower energy boundaries, as expected [34].

The effect of energy anisotropy α of high misorientation boundaries on AGG was examined, and the results of MC simulations were compared between low boundary energy anisotropy $\alpha = 0.1$ and 0.0, and between high boundary energy anisotropy $\alpha = 0.3$ and 0.4. The other conditions were fixed with sub-grains whose misorientations (θ) with the near-Goss grain were varied from 0.05° to 0.25°. Fig. 8a and b shows the plot of $R/\langle R\rangle$ vs. simulation time for $\alpha = 0.0$ and 0.1, respectively. For $\alpha = 0.0$ (Fig. 8a), all the slopes of the graph for $\theta = 0.05°$, 0.10°, 0.15°, 0.20° and 0.25° are negative except for the initial period of grain growth due to an initially given non-equilibrium condition. For $\alpha = 0.1$ (Fig. 8b), the slopes of the graphs for $\theta = 0.10°$, 0.15°, 0.20° and 0.25° are also negative. The slope for $\theta = 0.05$ is positive initially, but becomes negative after 200 MCS. The graphs for $\alpha = 0.0$ and 0.1 in Fig. 8 shows that under the condition of low energy anisotropy the near-Goss grain with sub-grains, even if the sub-grain boundaries have very low misorientation (≈0.05°), shrinks or AGG does not occur, which is in contrast with the case for $\alpha = 0.2$ shown in Fig. 6. These results imply that a significant anisotropy of grain boundary energy of matrix grains must exist in order for AGG to occur by sub-boundary-enhanced solid-state wetting.

Fig. 9a and b shows the plot of $R/\langle R\rangle$ vs. simulation time for $\alpha = 0.3$ and 0.4, respectively. The graphs in Fig. 9 are quite different from those of Fig. 8. For $\alpha = 0.3$ (Fig. 9a), the overall slopes of the graphs for $\theta = 0.05°$, 0.10° and 0.15° are positive. The slopes for $\theta = 0.20°$ and 0.25° become positive or negative, depending on the simulation period. For $\alpha = 0.4$ (Fig. 9b), the overall slopes for all θ values are positive and slightly higher than those in Fig. 9a. Compared with the graph for $\alpha = 0.2$ shown in Fig. 6, the graphs for $\alpha = 0.3$ and 0.4 in Fig. 9 show that under the condition of higher energy anisotropy the near-Goss grain with sub-boundaries of higher misorientation such as 0.15°, 0.20° and 0.25° can grow abnormally for $\theta = 0.05°$ and 0.10°. These results imply that the high energy anisotropy increases the threshold angle above which sub-boundaries induce AGG. For instance, the misorientation angles of sub-boundaries to induce AGG has to be lower than 0.15° for $\alpha = 0.2°$ and 0.20° for $\alpha = 0.4°$.

Figs. 6, 8 and 9 show that the energy anisotropy α in matrix grains and the sub-boundary misorientation θ inside the near-Goss grain are closely related to each other with respect to inducing AGG. In the case of low α (Fig. 8), the near-Goss grain for all θ values in the graph did not

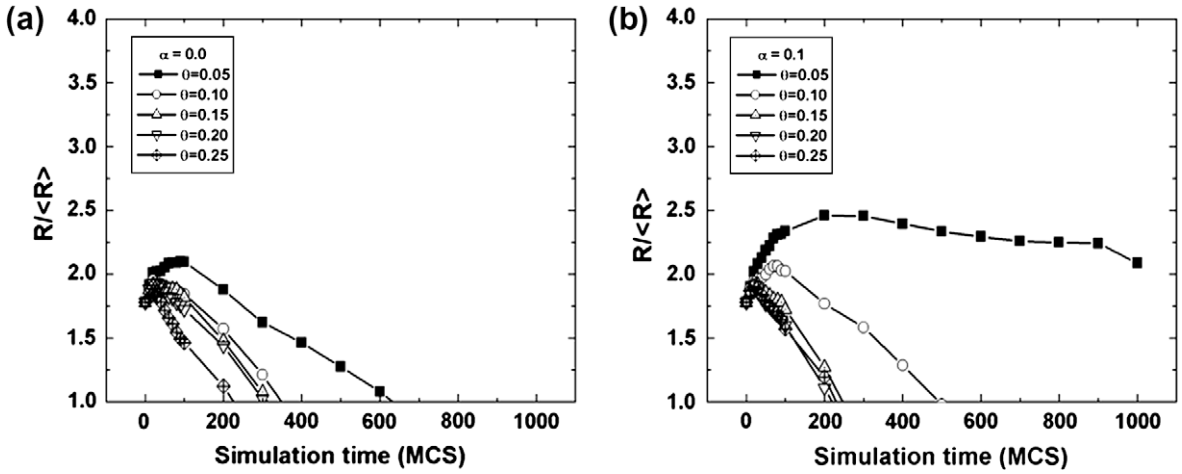

Fig. 8. Graphs of $R/\langle R\rangle$ vs. simulation time for the near-Goss grain with sub-grains and the sub-boundary misorientation $\theta = 0.05°$, 0.10°, 0.15°, 0.20° and 0.25° for (a) $\alpha = 0.0$ and (b) $\alpha = 0.1$.

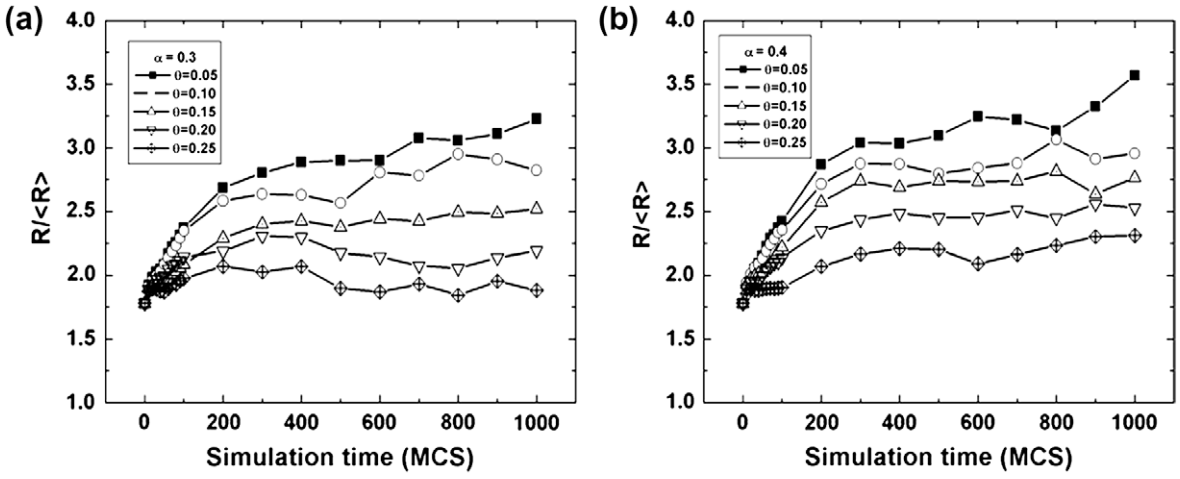

Fig. 9. Graphs of $R/\langle R\rangle$ vs. simulation time for the near-Goss grain with sub-grains and the sub-boundary misorientation $\theta = 0.05°$, 0.10°, 0.15°, 0.20° and 0.25° for (a) $\alpha = 0.3$ and (b) $\alpha = 0.4$.

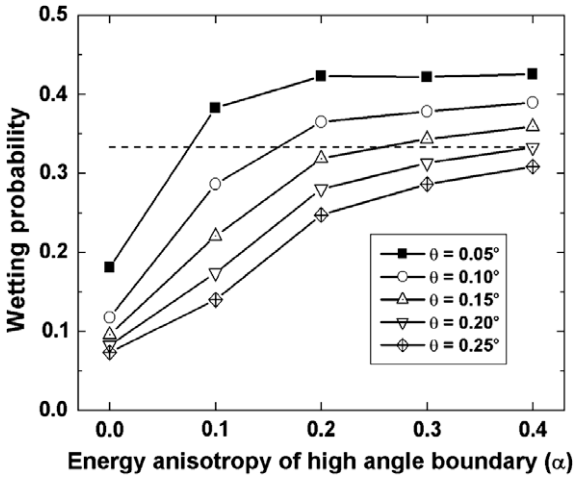

Fig. 10. The wetting probability as a function of the energy anisotropy α of high angle boundaries for $\theta = 0.05°$, 0.10°, 0.15°, 0.20° and 0.25°. The dotted line indicates the threshold wetting probability of 1/3 to continue abnormal grain growth by triple junction wetting.

exhibit AGG. In the case of high α, as in Fig. 9, however, the near-Goss grain for most θ values did show AGG. In the case of $\alpha = 0.2$ in Fig. 6, the near-Goss grain did not undergo AGG for high θ such as 0.20° and 0.25°, but exhibited sustained AGG at low θ values such as 0.05° and 0.10°.

In order to examine the correlation between θ, α and sub-boundary-enhanced solid-state wetting, the probability that wetting can occur at a given quadruple point as a function of the range of energies for high angle boundaries (as specified by α) was calculated by using the criterion for wetting at a quadruple point as follows [17,35]:

$$\text{wetting\_probability} = \frac{\sum_{i=1}^{N}\chi_i}{N}$$

$$\chi_i = \begin{cases} 1, & \text{if } \sum_{i=1}^{3}\theta_i < 180° \text{ and } \theta_i < 120° \\ 0, & \text{otherwise} \end{cases} \quad (4)$$

where N is the number of wetting trials and θ_1, θ_2 and θ_3, ranging from 0° to 180°, are the inner dihedral angles of a three-sided grain, as shown in Fig. 1b.

In order to calculate the probability of sub-boundary-enhanced wetting for various θ and α, grains "A" and "D" were assumed to share a sub-boundary of misorientation θ and the other boundary energies were determined by a weighted selection according to the boundary energy distribution for each condition as shown in Fig. 7. Based on Eq. (4), the wetting probabilities were calculated for sub-boundary misorientations, $\theta = 0.05°$, 0.10°, 0.15°, 0.20° and 0.25°, and for energy anisotropies, $\alpha = 0.0$, 0.1, 0.2, 0.3 and 0.4. The sub-boundary energies of misorientation θ were determined according to the dislocation model derived by Read and Shockley [26]. The calculated result is shown in Fig. 10. The wetting probability increases with decreasing sub-boundary energy and with increasing anisotropy of grain boundary energy, which corresponds to the MC simulation results.

If the wetting condition in Eq. (4) is satisfied at a quadruple point, the grain undergoes solid-state wetting along the triple line made by the three neighboring grains. The triple junction wetting continues until the wetting front reaches the next quadruple point. This new quadruple point has three additional triple lines, which are new candidates for wetting. If any of the three triple lines satisfies the wetting condition in Eq. (4), the wetting continues. The expected number of wetting events for a grain is three times the number of quadruple points multiplied by the probability of wetting. Therefore, if the wetting probability is higher than 1/3, it is likely that wetting events will continue during grain growth. The wetting probability of 1/3 is therefore the condition for AGG by solid-state wetting.

This wetting probability of 1/3 is indicated by a dotted line in Fig. 10. This suggests that the probabilities of wetting for $\theta = 0.05$ with $\alpha = 0.1$, $\theta = 0.05$ and 0.10 with $\alpha = 0.2$, and $\theta = 0.05$, 0.10 and 0.15 with $\alpha = 0.3$ and 0.4 were all higher than 1/3. All slopes under these conditions

in Figs. 6 and 9 are positive except for the slope for $\theta = 0.05$ with $\alpha = 0.1$, in which case the grain boundary energy anisotropy appears not to be high enough to sustain triple junction wetting. On the other hand, the probabilities of wetting for $\theta = 0.15$ with $\alpha = 0.2$ and 0.3, and $\theta = 0.20$ with $\alpha = 0.4$ were close to 1/3. The slopes under these conditions are close to zero. The probabilities of wetting for the other conditions of θ and α were lower than 1/3. Under these conditions the slopes are negative in Figs. 6 and 9. Therefore, when the wetting probability is higher than 1/3, the overall slope in Figs. 6, 8 and 9 is positive, indicating that AGG occurs.

3.3. Discussion

The simulation results suggest that a combination of low misorientation sub-boundaries with variation (anisotropy) in boundary energy of the matrix grains favors selective AGG of the grains that contain the low angle boundaries. In Fe–3% Si steel, Goss grains with an orientation of {1 1 0}<0 0 1> tend to be selected as an abnormally growing grain, producing a sharp Goss texture after secondary recrystallization. From a practical perspective, selective Goss AGG is the result of the particular choice of the process conditions, which include hot rolling, cold rolling, primary recrystallization and precipitation of grain growth inhibitors. After this process, if the Goss-oriented grains have sub-boundaries of low misorientation, the selective Goss AGG can occur with the final evolution of a sharp Goss texture. It is likely that sub-boundary formation in Goss grains depends on special processing conditions developed by each silicon steel production company that pursues the optimization to produce the sharp Goss texture after secondary recrystallization.

An important feature in Goss AGG in Fe–3% Si steel is that near the dissolution temperature of precipitates in Fe–3% Si steel Goss grains start to grow while growth of other grains is still inhibited by precipitates [36]. Therefore, the selective Goss AGG appears to be strongly correlated with dissolution of precipitates. In sub-boundary-enhanced wetting mechanism for selective Goss AGG, the role of precipitates is somewhat different from the previous suggestion. Near the dissolution temperature of precipitates, the precipitates on triple junctions or four-grain corners would coarsen or weaken faster than those on the other locations, such as the grain boundary plane and the matrix, due to kinetically fast diffusion at triple junctions or four-grain corners. This situation would allow Goss grains with sub-grain boundaries to grow extensively by sub-boundary-enhanced wetting whereas grain growth of the other grains is still inhibited by precipitates that have not yet coarsened.

Another important role of precipitates for inducing extensive Goss AGG in Fe–3% Si steel may be that they preserve high energy grain boundaries among the matrix grains during primary recrystallization and during heating to the secondary recrystallization temperature. Without precipitates, normal grain growth would occur extensively in Fe–3% Si during primary recrystallization and heating. After extensive normal grain growth most high energy grain boundaries would be replaced by low energy grain boundaries, as mentioned above. If the matrix grain boundaries are predominantly low energy, sub-boundary-enhanced solid-state wetting is not favored. In the presence of precipitates, however, normal grain growth is inhibited and the fraction of high energy boundaries in the matrix grains produced by primary recrystallization is maintained during primary recrystallization and heating, favoring the sub-boundary-enhanced solid-state wetting.

4. Conclusion

A parallel MC algorithm was used to simulate Goss AGG in Fe–3% Si steel via sub-boundary-enhanced solid-state wetting. If the Goss grain has sub-boundaries of very low misorientation, there is a high probability of solid-state wetting against matrix grains with moderately anisotropic grain boundary energy. AGG by sub-boundary-enhanced solid-state wetting was analyzed by calculating the probability of solid-state wetting, as dependent on sub-boundary misorientation and anisotropic boundary energy. The selective sharp Goss texture can evolve by AGG provided that only Goss grains contain sub-grains with very low misorientations. These low angle boundaries promote AGG by sub-boundary-enhanced solid-state wetting. This mechanism provides a possible explanation for the role of sub-boundaries previously observed in abnormally growing Goss grains in Fe–3% Si steel.

Acknowledgements

This work was financially supported by POSCO Technical Research Laboratories and also by the National Research Foundation of Korea (NRF) grant funded by the Korean government (MEST; No. M10600000159-06J0000-15910). The Intel Corporation is thanked for the provision of computing facilities. Discussions with colleagues under the auspices of the Computational Materials Science Network (CMSN) under DOE/OBES support have been invaluable. Use of facilities provided by the MRSEC at CMU under NSF grant number is DMR-0520425 is also gratefully acknowledged.

References

[1] Goss NP. Trans Am Soc Met 1935;23:511.
[2] Dillon SJ, Harmer MP. Mater Sci Forum 2007;558–559:1227.
[3] Dillon SJ, Harmer MP. Acta Mater 2007;55:5247.
[4] Jo W, Kim DY, Hwang NM. J Am Ceram Soc 2006;89:2369.
[5] Ferry M, Humphreys FJ. Acta Mater 1996;44:1271.
[6] Harase J, Shimizu R, Takashima K, Watanabe T. Trans ISIJ 1987;27:965.
[7] May JE, Turnbull D. Trans TMS-AIME 1958;212:769.
[8] Harase J, Shimizu R, Dingley DJ. Acta Metall Mater 1991;39:763.
[9] Ushigami Y et al. Mater Sci Forum 2004;467–470:853.

[10] Rajmohan N, Szpunar JA, Hayakawa Y. Acta Mater 1999;47:2999.
[11] Etter AL, Baudin T, Penelle R. Scripta Mater 2002;47:725.
[12] Morawiec A. Scripta Mater 2000;43:275.
[13] Hwang NM. J Mater Sci 1998;33:5625.
[14] Park H et al. J Appl Phys 2004;95:5515.
[15] Lee SB, Hwang NM, Han CH, Yoon DY. Scripta Mater 1998; 39:825.
[16] Ko KJ, Cha PR, David S, Hwang NM. Acta Mater 2009;57:838.
[17] Lee DK, Ko KJ, Lee BJ, Hwang NM. Scripta Mater 2008;58:683.
[18] Ko KJ, Park JT, Kim JK, Hwang NM. Scripta Mater 2008;59:764.
[19] Smith CS. Trans Amer Inst Min Met Eng 1948;175:15.
[20] Park HK, Kim SD, Park SC, Park JT, Hwang NM. Scripta Mater 2010;62:376.
[21] Ushigami Y et al. J Mater Eng 1991;13:113.
[22] Suzuki S, Ushigami Y, Suga Y, Takahashi N. Mater Sci Forum 1996;204–206:575.
[23] Dorner D, Lahn L, Zaefferer S. Mater Sci Forum 2004;467–470:129.
[24] Dorner D, Zaefferer S, Raabe D. Acta Mater 2007;55:2519.
[25] Wright SA et al. Potts-model grain growth simulations: parallel algorithms and applications. Albuquerque (NM): Sandia National Labs; 1997.
[26] Read WT, Shockley W. Phys Rev 1950;78:275.
[27] Saylor DM, Fridy J, El-Dasher BS, Jung KY, Rollett AD. Metall Mater Trans 2004;35A:1969.
[28] Wolf D. Philos Mag A 1990;62:447.
[29] Brandon DG. Acta Metall 1966;14:1479.
[30] Rollett AD. Mater Sci Forum 2005;495–497:1171.
[31] Miodownik M, Godfrey AW, Holm EA, Hughes DA. Acta Mater 1999;47:2661.
[32] Rollett AD, Srolovitz DJ, Anderson MP. Acta Metall 1989;37:1227.
[33] Rios PR. Acta Metall Mater 1992;40:2765.
[34] Gruber J, George DC, AKuprat AP, Rohrer GS, Rollett AD. Scripta Mater 2005;53:351.
[35] Hwang NM, Lee SB, Kim DY. Scripta Mater 2001;44:1153.
[36] Ushigami Y et al. Mater Sci Forum 1994;157–162:1081.